

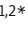








ARTICLE

Coordinated neurostimulation promotes circuit rewiring and unlocks recovery after spinal cord injury

Valérie Van Steenberghe^{1,2} , Laura Burattini^{1,2*} , Michelle Trumpp^{1,2*} , Julie Fourneau^{1,2} , Almir Aljović^{1,2,4} , Maryam Chahin^{1,2,4} , Hanseul Oh^{1,2,4} , Marta D'Ambra^{1,2} , and Florence M. Bareyre^{1,2,3} 

Functional recovery after incomplete spinal cord injury depends on the effective rewiring of neuronal circuits. Here, we show that selective chemogenetic activation of either corticospinal projection neurons or intraspinal relay neurons alone led to anatomically restricted plasticity and little functional recovery. In contrast, coordinated stimulation of both supraspinal centers and spinal relay stations resulted in marked and circuit-specific enhancement of neuronal rewiring, shortened EMG latencies, and improved locomotor recovery.

Introduction

While the regenerative capacity of injured axons of the central nervous system (CNS) is limited, the formation of intraspinal detour circuits has been shown to contribute to spontaneous motor recovery after incomplete spinal cord injury (SCI; [Bareyre et al., 2004](#); [Courtine et al., 2008](#); [Ueno et al., 2012](#); [Zörner et al., 2014](#); [Jacobi and Bareyre, 2015](#); [Raineteau and Schwab, 2001](#)). A paradigmatic detour circuit is formed by injured corticospinal tract (CST) hindlimb projections that use long propriospinal neurons (LPSNs) located in the cervical spinal cord to relay information around the thoracic lesion to the lumbar spinal cord. We and others have previously shown that the formation of corticospinal detour circuits depends on neuronal activity ([Bradley et al., 2019](#); [Brommer et al., 2021](#); [Chen et al., 2018](#)) as silencing of long propriospinal interneurons leads to decreased circuit rewiring and diminished functional recovery ([Bradley et al., 2019](#)). This has raised the possibility that the modulation of neuronal activity could be leveraged for therapeutic purposes.

Indeed, a number of studies have shown that increasing neuronal activity in different models of CNS injuries can promote some level of functional recovery ([Deng et al., 2021](#); [Carmel et al., 2013](#); [Bachmann et al., 2013](#); [Chen et al., 2018](#); [Kathe et al., 2022](#)). Clinical studies have also demonstrated the beneficial effects on motor recovery of combined corticospinal tract via transcranial magnetic stimulation and lower spinal circuit stimulation using peripheral nerve stimulation ([Shulga et al., 2021](#); [Pohjonen et al., 2021](#); [Vaalto et al., 2021](#); [Pulverenti et al.,](#)

[2021](#)). However, it is still unclear how to best design efficient neurostimulation therapies above the lesion site and which circuit components they should target to enhance the functional gain that is currently still limited. The proper understanding of the relative contribution of supraspinal centers and spinal relay stations to support the rewiring of preidentified adaptive circuits and whether the coordinated stimulation of those different circuit elements yields synergistic or antagonistic effects is also still unresolved.

Here, we therefore used the targeted expression of designer receptors exclusively activated by designer drugs (DREADDs) in combination with administration of clozapine N-oxide (CNO) to induce the long-lasting non-invasive neuromodulation of defined neuronal circuit elements ([Roth, 2016](#); [Van Steenberghe and Bareyre, 2021](#); [Bradley et al., 2019](#); [Hilton et al., 2016](#)). By using viral tracing methods, we assessed circuit rewiring after injury and found that while supraspinal stimulation induced synaptogenesis along newly established axonal projections, it was unable to direct those new synapses onto spared intraspinal neurons, and thus no improvement in functional recovery was observed. Stimulation of spared intraspinal neurons, shown to be mainly a ZFH3-positive subpopulation of V2a spinal neurons, however, attracted growing supraspinal axons, and therefore strengthened the formation of the detour circuit, ultimately responsible for a significant but limited improvement in motor recovery. Coordinated stimulation of both the

¹Institute of Clinical Neuroimmunology, University Hospital, LMU Munich, Munich, Germany; ²Biomedical Center Munich (BMC), Faculty of Medicine, LMU Munich, Planegg-Martinsried, Germany; ³Munich Cluster of Systems Neurology (SyNergy), LMU Munich, Munich, Germany; ⁴Graduate School of Systemic Neurosciences, LMU Munich, Planegg-Martinsried, Germany.

*L. Burattini and M. Trumpp contributed equally to this paper. Correspondence to Florence M. Bareyre: florence.bareyre@med.uni-muenchen.de.

© 2022 Van Steenberghe et al. This article is distributed under the terms of an Attribution–Noncommercial–Share Alike–No Mirror Sites license for the first six months after the publication date (see <http://www.rupress.org/terms/>). After six months it is available under a Creative Commons License (Attribution–Noncommercial–Share Alike 4.0 International license, as described at <https://creativecommons.org/licenses/by-nc-sa/4.0/>).

supraspinal and intraspinal circuit components led to synergistic modulation of the detour circuit and vastly enhanced motor recovery owing to adapted motion patterns as evaluated by kinematic analysis. The anatomical changes that form the basis for functional recovery were further validated by EMG recordings and transcriptome analysis. Our data indicate that our coordinated stimulation approach can not only induce synergistic benefits for motor behavior after SCI but that targeted neuromodulation therapies can be used to guide circuit remodeling between defined neuron populations.

Results

Chemogenetic stimulation of corticospinal neurons promotes synapse maturation

We first examined the effects of the selective stimulation of the supraspinal (presynaptic) circuit element on detour circuit formation by stereotactically injecting an rAAV expressing an activating DREADD (hM3Dq) under a neuronal promoter to the layer V of the cortex (Fig. 1, A and B). Using c-fos expression as a read-out of neuronal activity (Dragunow and Faull, 1989; Bullitt, 1990; Botterill et al., 2021), we first demonstrate that application of CNO to uninjured mice does not only increase the stimulation of DREADD-expressing corticospinal neurons but also of their neighboring neurons, indicating an increase in cortical network activation (Fig. 1 C), while no such stimulation was observed by repetitive CNO administration alone (Fig. S1). To prevent inhibition of collateral growth upon stimulation of the transected corticospinal tract (Hilton et al., 2022), we started our stimulation paradigm from 7 d postinjury (dpi) when most collaterals have sprouted (Lang et al., 2012; Fig. S2, A–M). When activating corticospinal projection neurons in mice with a midthoracic spinal cord injury, we observed an increase in the number and maturation of synapses along CST collaterals as indicated by the presence of presynaptic Vglut1/2 positive vesicles (Fig. 1 D and Fig. S2). No effects on the number of exiting CST collaterals were observed (Fig. S2 C). However, this enhanced synaptogenesis did not translate to an increased formation of detour circuits as the CST contacts onto LPSNs or other spinal neurons remain unchanged (Fig. 1, E and F; and Fig. S2 D). Indeed, the percentage of varicosities colocalizing with Homer, a postsynaptic scaffolding protein, was not altered (Fig. S2 L). Stimulation of corticospinal neurons thus boosts the maturation state of synapses mainly through the maturation of presynaptic varicosities along the collaterals without affecting the number of synaptic contacts onto spinal neurons and as such has no effect on circuit rewiring.

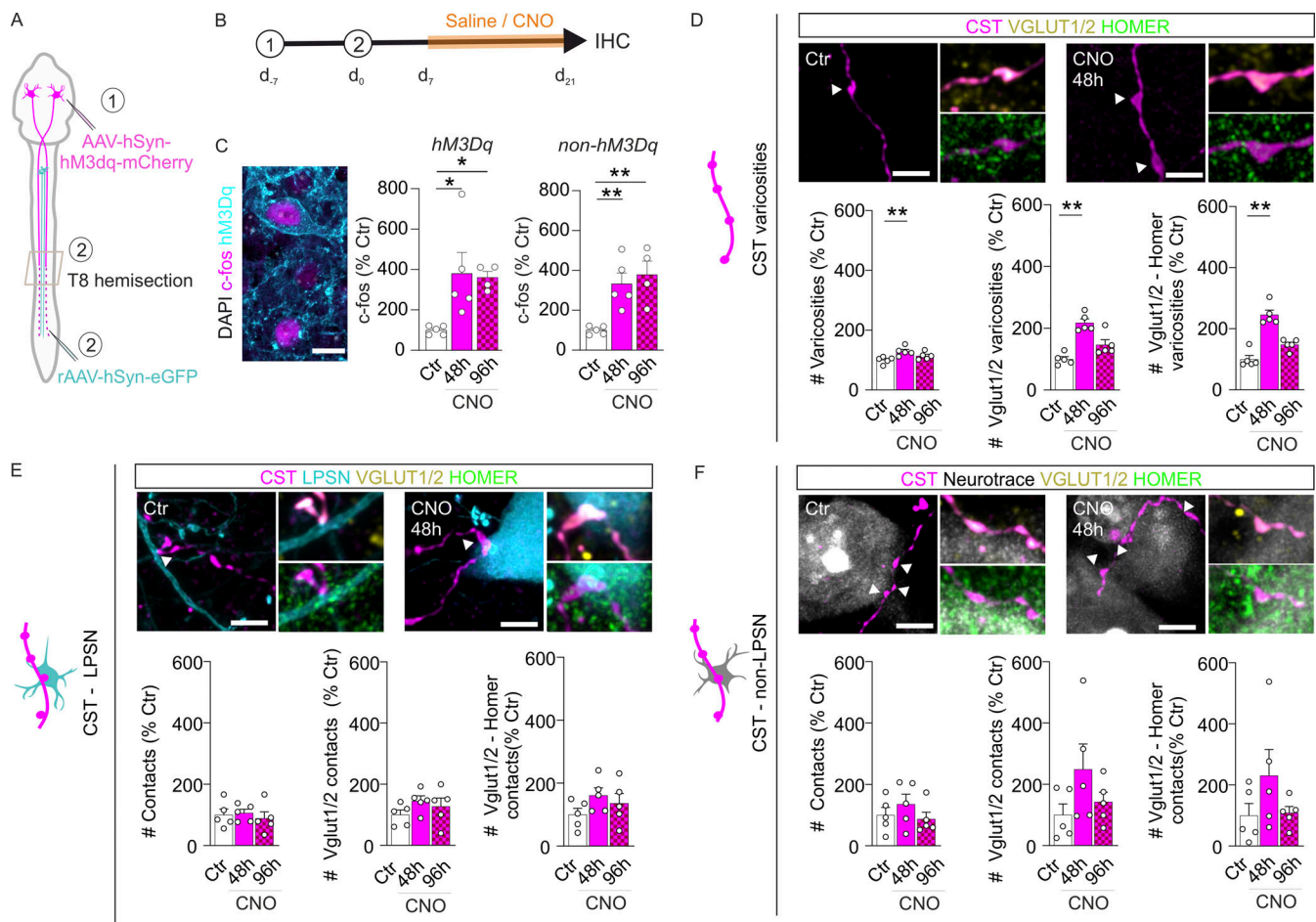
Selective chemogenetic stimulation of LPSNs leads to anatomically restricted alterations of circuit rewiring

We next set out to determine the effects of selective stimulation of the spinal (postsynaptic) circuit element. To selectively activate cervical LPSNs, we combined cervical injections of an rAAV allowing the CRE-dependent expression of an activating DREADD in neurons with lumbar injections of a retrograde AAV expressing the CRE recombinase (Fig. 2, A and B). Indeed, DREADD-expressing LPSNs showed a significant increase in

c-fos expression, while we observed no indication of increased spinal network activation in uninjured mice (Fig. 2 C). After spinal cord injury, repetitive LPSN stimulation led to a marked increase in the number and maturation state of CST contacts onto LPSNs while only minor changes to the overall number and maturation state of presynaptic varicosities along CST collaterals were observed (Fig. 2, D and E; and Fig. S2). Interestingly, the number of contacts of CST with neighboring intraspinal neurons that did not express the DREADDs remained unchanged (Fig. 2 F). These results indicate that circuit-specific rewiring can be achieved by targeted spinal neurostimulation and that no aberrant contacts are formed on non-targeted spinal neurons. This is in line with our earlier observation that these non-targeted neurons did not increase their activity (Fig. 2 C). Taken together, our results therefore indicate that chemogenetic activation of the lesioned supraspinal circuit component—here the hindlimb CST—prompts synapse formation along regrowing CST collaterals but lacks cues to specifically target spinal relay neurons. In contrast, activation of spinal relay stations—here LPSNs—can attract CST contacts to LPSNs but offers only limited stimulation of CST synaptogenesis.

Coordinated stimulation of corticospinal projection neurons and LPSNs enhances circuit rewiring

Our results suggest that a coordinated stimulation of supraspinal and spinal circuit elements could have synergistic effects on circuit rewiring. We therefore combined both supraspinal and spinal stimulation approaches and recorded the effects on the different circuit elements after incomplete midthoracic spinal cord injury (Fig. 3 A). Our results demonstrated that this coordinated stimulation indeed led to both an increase in the number of presynaptic varicosities along the CST (Fig. 3 B) as well as a marked (more than threefold) increase in the number of mature synaptic contacts of these CST collaterals onto LPSNs (Fig. 3 C and Fig. S2). Notably, despite the increase in CST synaptogenesis, no change in the number of CST contacts onto non-activated spinal neurons was detected (Fig. 3 D), indicating that the targeted stimulation approach boosts neuronal rewiring in a circuit-specific manner. The increase in double positive synaptic contacts (Vglut and Homer) is furthermore not linked to activity-induced Homer expression as Homer levels, both at the protein level as well as mRNA level, were not increased (Fig. S2 M). To elucidate whether the CST targets a specific subpopulation of LPSNs and determine whether this specificity is altered upon our combined stimulation paradigm, we further looked into cardinal classes of spinal neurons. Using V2a markers NFIB and ZFHX3, we found that 70% of LPSNs are V2a positive neurons, all expressing the transcription factor ZFHX3, independent of the treatment group (Fig. 3 F). When we quantified the nature of the contacted LPSN, we found that most contacted neurons are ZFHX3 positive (Fig. 3 G). Interestingly, there is no change in the type of neuron contacted between the treatment groups. Combined stimulation of the CST and LPSNs thus leads to a significant increase in synaptic contacts and targets a similar subpopulation of LPSNs as in endogenous detour wiring.



Coordinated stimulation of corticospinal projection neurons and LPSNs shortens EMG latency and increases synapse transcriptomic profiles

To further validate that our coordinated stimulation strategy can lead to functionally meaningful improvement of supraspinal-to-spinal connectivity, we performed EMG recordings after cortical stimulation (Fig. 4, A and B). Our results show both a significant decrease in the latency as well as a trend toward a higher amplitude of the EMG response (Fig. 4 C). Finally, assessing the transcriptome of the cervical spinal cord upon combined stimulation indicates clear clustering of both experimental groups (Fig. 4, D and E; and Fig. S3). Gene ontology (GO)-enrichment analysis leads to an enrichment of genes involved in synaptic functions (Fig. 4, F and G), validating our anatomical circuit analysis. Taken together, our study established that the coordinated stimulation of supraspinal projection and spinal relay neurons induced circuit-specific neuronal rewiring that resulted in

more efficient connectivity between supraspinal motor control and lumbar motoneurons.

Coordinated stimulation of corticospinal projection neurons and LPSNs improves locomotor recovery

Finally, we wanted to assess the effects of the distinct stimulation paradigms on the recovery of locomotor function after spinal cord injury (Fig. 5 A). For this purpose, we first ensured that repetitive injections of CNO did not affect the stepping abilities of uninjured mice neither in the absence of DREADDs nor upon DREADD expression in the hindlimb CST, LPSNs, or both neuronal populations (Fig. S4 A). We also verified that acute activation did not alter “in-cage behavior” (grooming and scratching) of these mice over prolonged periods of time (Fig. S4, B and C). We also confirmed that all groups had similar lesion volumes and similar behavioral performance before and acutely after injury (Fig. S4, D and E). We then assessed the locomotor recovery of the distinct stimulation paradigms in injured

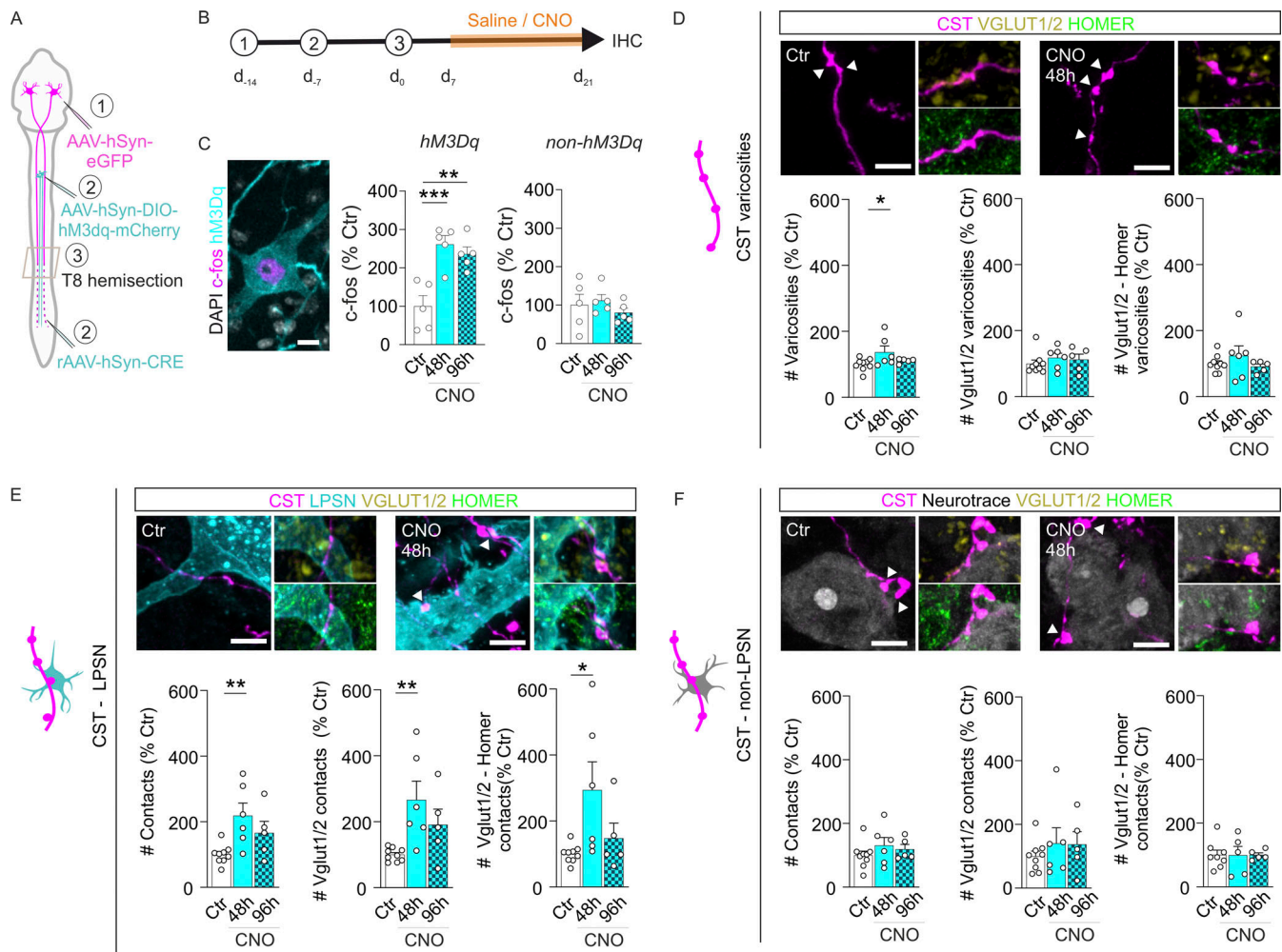


Figure 2. Selective chemogenetic stimulation of LPSNs leads to anatomically restricted alterations of circuit rewiring. (A) Schematic overview of in vivo surgical interventions for stimulating postsynaptic long propriospinal neurons. (B) Timeline for surgeries and i.p. injections of saline and CNO. (C) Confocal recording of c-fos expression 90 min after final saline/CNO injections. Quantification of c-fos expression in hM3Dq-positive neurons and non-hM3Dq cells ($n = 5$ mice). (D) Quantification of overall CST varicosity, Vglut1/2-positive synapses and Vglut1/2-Homer-positive synapses ($n = 5$ mice). (E) Quantification of CST contact density onto LPSNs, Vglut1/2-positive contacts, and Vglut1/2-Homer-positive contacts ($n = 5$ mice). (F) Quantification of CST contact density onto non-LPSN neuronal somas, Vglut1/2-positive contacts, and Vglut1/2-Homer-positive contacts ($n = 5$ mice). Data are represented with the individual biological replicates, the mean and error bars represent the SEM. Scale bars, 10 μm (C), 5 μm (D–F). P values were calculated with one-way ANOVA and Dunnett's multiple corrections (C–F). *, $P < 0.05$; **, $P < 0.01$; ***, $P < 0.001$.

mice using an irregular ladder test, which requires step-length adaptations and therefore assesses fine paw placement under supraspinal control (Fig. 5 B; Bradley et al., 2019; Loy and Bareyre, 2019; Liebetanz and Merkle, 2006). We calculated the percentage of recovery between the number of foot faults at 21 dpi and the number of foot faults at 3 dpi. We observed that while stimulation of the CST alone did not alter the performance of mice after injury, the stimulation of LPSNs alone led to a moderate improvement of motor recovery in line with the increased CST–LPSN contacts observed in this paradigm (Fig. 5, C and D). Notably, the coordinated supraspinal and spinal stimulation led to a further and significant amelioration of motor performance that exceeded the improvement observed in any of the isolated stimulation protocols (Fig. 5 E). To further determine how the different stimulation paradigms affected the locomotion pattern, we used motion kinematic analysis to

understand if the improved motor function arises from novel walking patterns (Fig. 5 F; Aljovic et al., 2022). Stimulation of supraspinal centers alone did not change kinematic parameters (Fig. 5, G and H), while LPSN stimulation alone induced a distinct walking pattern (Fig. 5, I and J; and Fig. S5). Activation of propriospinal neurons thus not only improved locomotion after acute stimulation as shown previously (Brommer et al., 2021) but activity-induced changes in circuit wiring upon repetitive stimulation can sustain recovered and adaptive motion patterns. Finally, when evaluating kinematic parameters in response to coordinated stimulation of the hindlimb CST and LPSNs, we observed marked changes (Fig. 5, K and L; and Fig. S5) indicating robust adaptations of the walking pattern that go beyond the effects induced by any isolated stimulation paradigm. In particular, the dragging percentage is significantly decreased, which further results in altered joint parameters

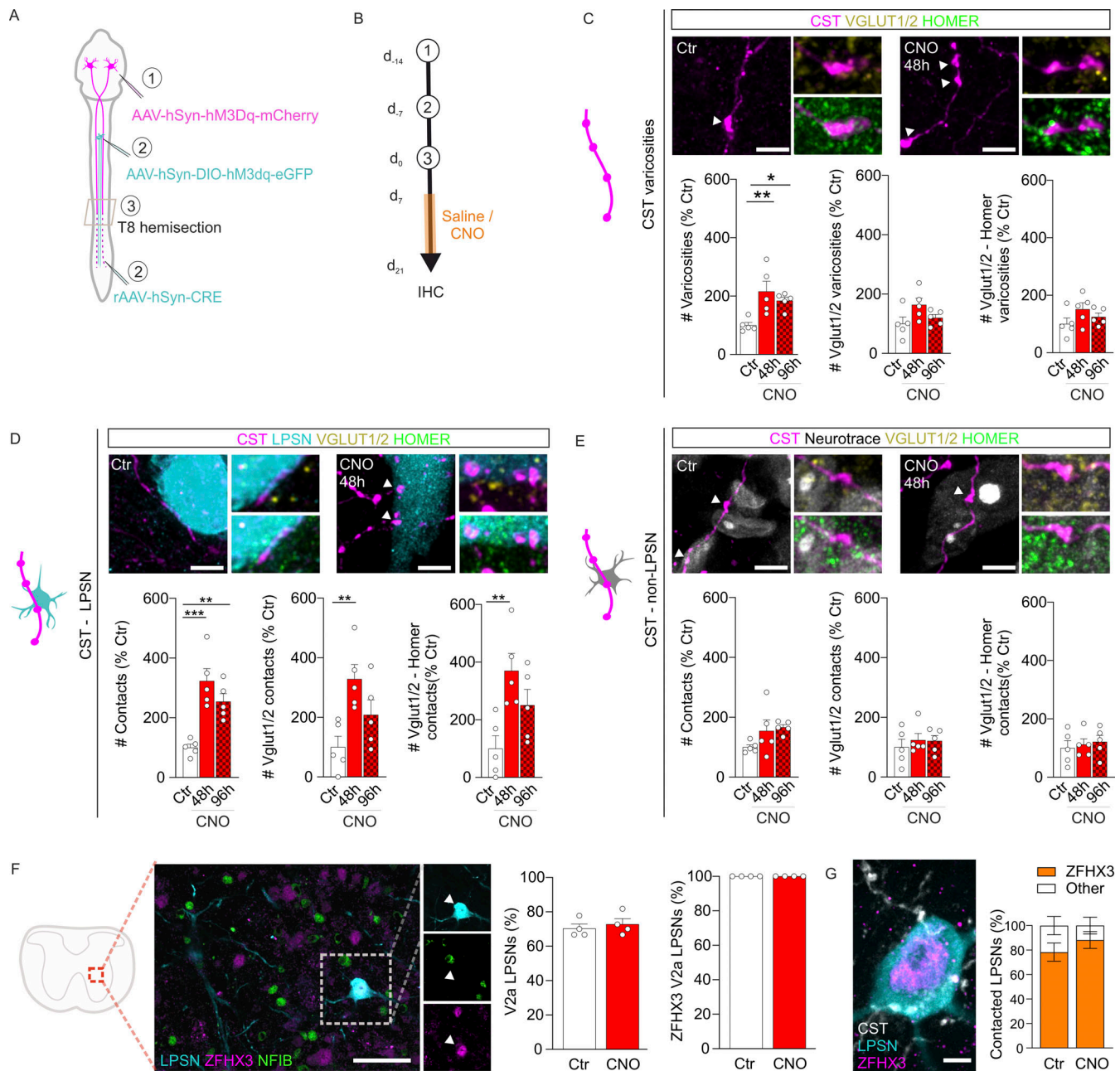


Figure 3. Coordinated stimulation of corticospinal projection neurons and LPSNs enhances circuit rewiring. (A and B) Schematic representation (A) and timeline (B) of in vivo surgical interventions for stimulating both pre- and postsynaptic circuit components. (C) Quantification of overall CST varicosities, Vglut1/2-positive synapses, and Vglut1/2-Homer-positive synapses (n = 5 mice). (D) Quantification of CST contacts onto LPSNs, Vglut1/2-positive contacts, and Vglut1/2-Homer-positive contacts (n = 5 mice). (E) Quantification of CST contacts onto non-LPSN neuronal somas, Vglut1/2-positive contacts, and Vglut1/2-Homer-positive contacts (n = 5 mice). (F) Overview of the ventral spinal cord with LPSNs stained for ZFH3 and NFIB and quantification of V2a LPSNs and the number of ZFH3 positive V2a LPSNs (n = 4 mice). (G) CST contacting a ZFH3 positive LPSN and quantification of the type of contacted LPSNs (n = 4 mice). Data are represented with the individual biological replicates and the mean and error bars represent the SEM. Scale bars, 5 μ m (C–E), 50 μ m (F). P values were calculated with one-way ANOVA and Dunnett's multiple corrections (C–F) and unpaired t test (F and G). *, P < 0.05; **, P < 0.01; ***, P < 0.001.

such as hip joint flexion. We also performed catwalk analysis and quantified gait parameters during spontaneous walking (Fig. 5 M). Here, we saw that the coupling between forelimbs and hindlimbs is specifically altered (Fig. 5, M and N). This is in line with the fact that most contacted LPSN relay neurons following SCI are ZFH3-positive (Fig. 3 G) and, therefore, a subpopulation of V2a neurons known to project to motor

neuron centers and involved in fore- and hindlimb-coordinated motor behavior. Thus, concomitant with the lack of circuit changes, stimulation of corticospinal tracts does not alter motor recovery or kinematic patterns. Stimulation of LPSNs however led to targeted synaptogenesis and is sufficient to induce a small but significant improvement in motor recovery linked to altered stepping patterns. Finally, the coordinated stimulation

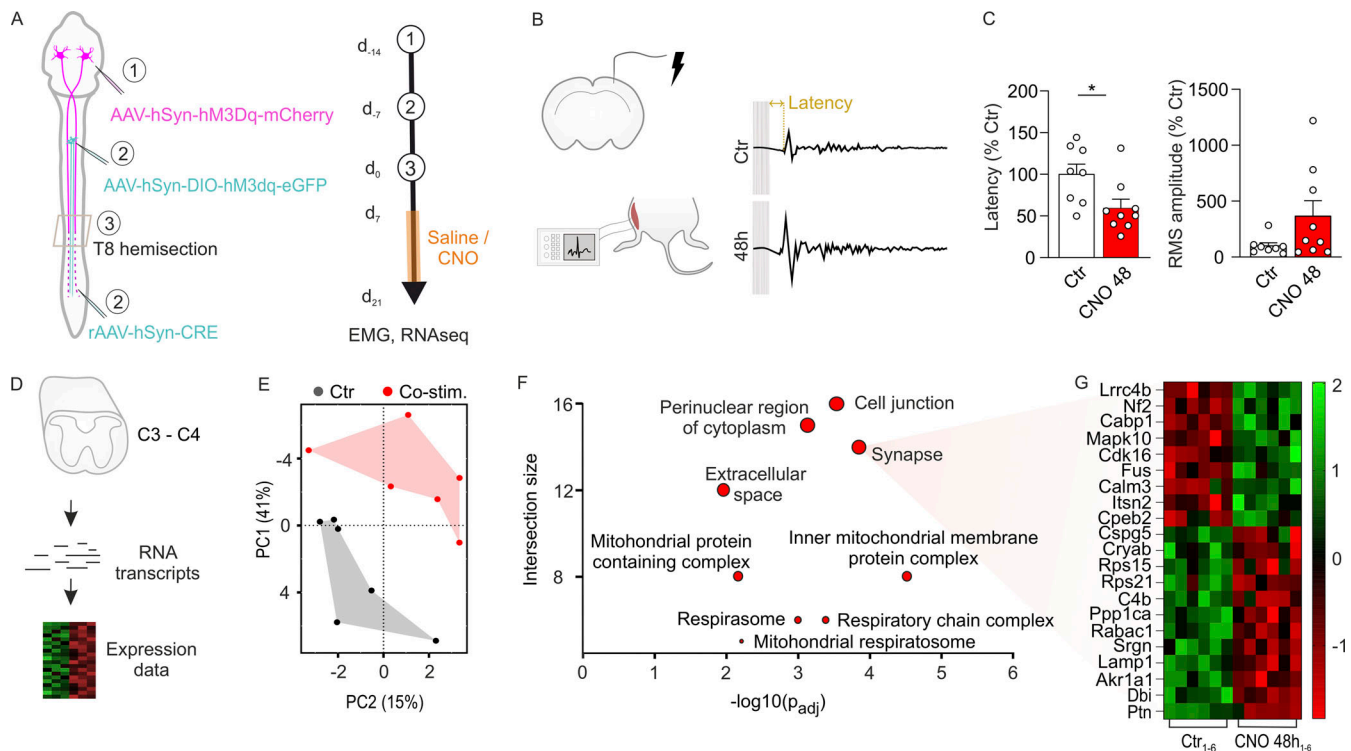


Figure 4. Coordinated stimulation of corticospinal projection neurons and LPSNs shortens EMG latency and increases synapse transcriptomic profiles. (A) Schematic representation and timeline of in vivo surgical interventions for stimulating both pre- and post-synaptic circuit components. (B) Schematic overview of the EMG setup and examples of EMG traces for both treatment groups. (C) Quantification of latency and root-mean-square amplitude (n = 8–9 mice). (D) Schematic overview of RNA sequencing. (E) PCA analysis of RNA sequencing data (n = 6 mice per group). (F) GO term enrichment analysis plotted as fold change and representation of the number of genes corresponding to the classification as an intersection size. (G) Heatmap of differentially expressed genes related to the GO classification synapse. Data are represented with the individual biological replicates, the mean and error bars represent the SEM. P values were calculated with unpaired *t* test (C, latency) and Mann-Whitney test (C, RMS amplitude). *, P < 0.05; **, P < 0.01; ***, P < 0.001.

pattern induced the largest change in detour circuit wiring and motor recovery owing to improved walking patterns.

Discussion

It is established that the formation of detour circuits after SCI is not only required for spontaneous recovery but that they can also be harnessed to modulate motor recovery (Bareyre et al., 2004; Courtine et al., 2008; Ueno et al., 2012; Zörner et al., 2014; Granier et al., 2020; van den Brand et al., 2012; Bonizzato et al., 2021; Brommer et al., 2021; Jacobi et al., 2015). The formation of detour circuits is based on neuroplasticity, and as such, strategies to enhance synaptogenesis are a promising strategy to alleviate motor impairment. To this end, increasing neuronal activity with epidural stimulation, deep brain electrical stimulation, or optogenetics has been shown to improve functional recovery both in rodents and humans (Deng et al., 2021; Carmel et al., 2013; Bachmann et al., 2013; Angeli et al., 2018; Wagner et al., 2018). It remains however unclear whether targeted neuromodulation of specific neuron populations can be used to enhance targeted circuit rewiring and functional recovery. In our study, we elucidate the effects of repeated supraspinal and intraspinal stimulation, or the combination thereof, on circuit remodeling and functional recovery after an incomplete dorsal hemisection.

Chemogenetic stimulation of the presynaptic component, in our study the severed hindlimb CST, primes synaptogenesis along newly established axonal projections but does not allow the formation of new contacts onto spared relay neurons. The increase in boutons along the collaterals is thus mainly linked to presynaptic maturation rather than an increase in synaptic contact formation. We further show that this stimulation paradigm in the brain does neither increase the recovery potential nor the adaptations in the gait pattern of recovering mice. This is interesting, as previous reports have shown that brain electrical or optogenetic stimulation, techniques that directly depolarize neurons, can improve motor skills (Deng et al., 2021; Carmel and Martin, 2014; Carmel et al., 2014). Chemogenetic constructs rather act by reducing the threshold for action potential propagation by intracellular signaling cascades (Alexander et al., 2009). This distinct mode of action might explain these differences and might also limit the risk of inducing strong involuntary movements such as reported using electro- or optogenetic stimulation (Deng et al., 2021; Bonizzato et al., 2021). Therefore, it appears that the chemogenetic stimulation of the severed hindlimb CST leads to synaptic priming of new axonal sprouts, which could potentially be used to further target intraspinal neurons in appropriate conditions. Care should be taken while designing a chemogenetic stimulation paradigm for neurons with transected axons, however, as stimulation during the

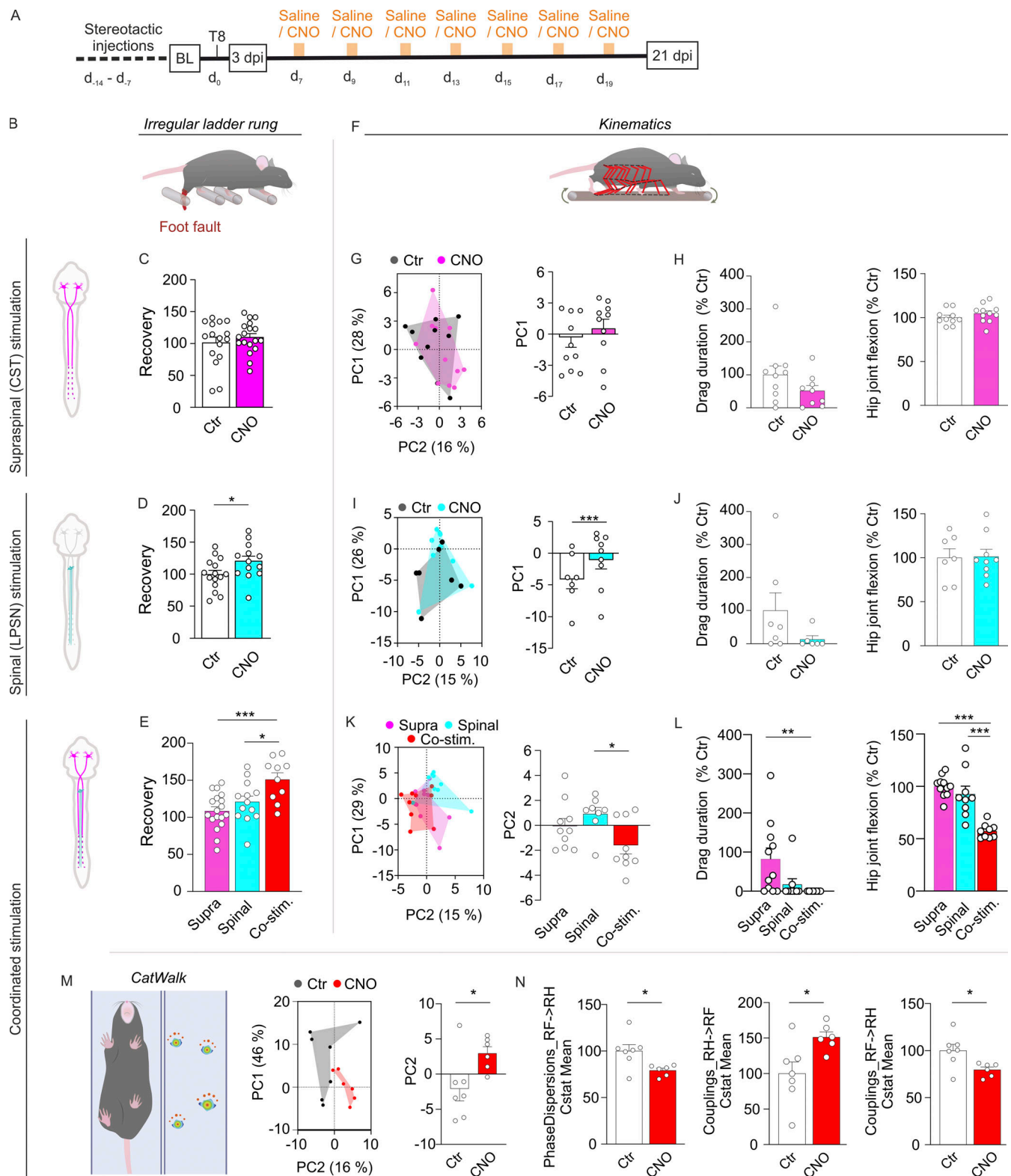


Figure 5. Coordinated stimulation of corticospinal projection neurons and LPSNs improves locomotor recovery. (A) Timeline of behavior experiments. (B) Schematic representation of the irregular horizontal ladder rung. (C) Quantification of the recovery between 3 and 21 dpi after hindlimb CST stimulation ($n = 16$ –18 mice). (D) Quantification of recovery ($n = 13$ –15 mice). (E) Comparison of the recovery gain between all treatment groups between 3 and 21 dpi ($n = 10$ –13 mice). (F) Schematic overview of the treadmill and corresponding kinematic parameter extraction. (G) PCA analysis of kinematic parameters deduced from the recovering animals after CST stimulation and quantification of PC 1 ($n = 10$ –11 mice). (H) Quantification of drag duration and hip joint flexion. (I) PCA analysis of kinematic parameters deduced from the recovering animals after LPSN stimulation and quantification of PC 1 ($n = 7$ –9 mice). (J) Quantification of drag duration and hip joint flexion. (K) PCA analysis of kinematic parameters deduced from the recovering animals at 21 dpi and quantification of PC2 ($n = 9$ –10

mice). **(L)** Quantification of drag duration and hip joint flexion. **(M)** Schematic representation of Catwalk and PCA analysis of the gait parameters obtained from recovering animals after coordinated CST and LPSN stimulation with quantification of PC2 ($n = 6-7$ mice). **(N)** Quantification of phase dispersion and couplings between the right hind- and forelimb ($n = 6-7$ mice). Error bars represent the SEM. Data are represented with the individual biological replicates, the mean and error bars represent the SEM. P values were calculated with a Mann-Whitney test (C and J), unpaired *t* test (D, H, M, and N), one-way ANOVA and Tukey's (E) or Dunn's (K and L) multiple corrections, and a mixed effects analysis with Tukey's multiple corrections (G and I). *, $P < 0.05$; **, $P < 0.01$; ***, $P < 0.001$.

collateral growth phase led to a decrease in exiting collaterals. This is in line with the study by [Hilton et al. \(2022\)](#), which showed that distinct transcriptional programs in neurons either induce regeneration or synaptogenesis, but presynaptic active zones inhibit axonal growth.

It was previously shown that chemogenetic silencing of cervical excitatory neurons, including LPSNs, after SCI results in reduced synaptogenesis and deterioration of motor skills ([Bradley et al., 2019](#)). While this study clearly demonstrates the role of neuronal activity in the spontaneous postinjury formation of detour circuits and ensuing functional recovery, whether repetitively increasing activity in LPSNs could ameliorate functional outcomes is still unclear. Recently, [Brommer et al. \(2021\)](#) elegantly demonstrated that hindlimb locomotion after SCI can be improved by acute chemogenetic activation of propriospinal neurons at the thoracic level. While the functional performance acutely after CNO administration was clearly better, it was still unclear whether repetitive activation of LPSNs can enhance circuit rewiring. Here, we show that repetitive stimulation of cervical LPSNs directs contact formation onto LPSN and ameliorates functional recovery chronically following SCI. Importantly, the absence of aberrant synaptic contact formation onto non-LPSN spinal neurons illustrates the specificity of our stimulation paradigm and suggests that this targeted strategy could be a meaningful way to reduce unwanted side effects. Thus, although cervical LPSNs only represent a small fraction of the total neuronal population in the spinal cord, targeted neuromodulation of these neurons can drive spinal circuitry rewiring and functional recovery after SCI.

We hypothesized that synaptic priming of the hindlimb CST upon stimulation in combination with the activation of LPSNs could lead to further circuit rewiring and unlock motor recovery. Indeed, the coordinated stimulation did not only enhance synaptogenesis and maturation between the supraspinal and intraspinal neuron populations but also further enhanced motor recovery owing to the altered walking pattern as assessed with kinematic parameter extraction. Taken together, our results are in line with an earlier study combining deep brain stimulation of the midbrain with epidural electrical stimulation in rats. Here, the researchers have similarly shown synergistic outcomes in terms of stepping abilities ([Bonizzato et al., 2021](#)). While this study shows that costimulation can be used to enhance stepping acutely upon activation, we further demonstrate the therapeutic potential of coordinated activation to strengthen circuit rewiring, ultimately leading to enhanced locomotion.

Harnessing preserved propriospinal neurons to ameliorate functional recovery after SCI in detour circuit formation has been extensively studied ([Bareyre et al., 2004](#); [Courtine et al., 2008](#); [Jacobi et al., 2015](#); [Ueno et al., 2012](#)). However, it remained unclear if—and which—specific subpopulation of neurons was

targeted. As the exiting CST collaterals mainly target excitatory neurons ([Bradley et al., 2019](#); [Bareyre et al., 2004](#)), we investigated whether the contacted LPSNs are the main subpopulation of V2a neurons. Indeed, 70% of our targeted LPSNs were V2a neurons, exclusively expressing ZHFX3 rather than NFIB markers for long- and short-projecting V2a neurons, respectively ([Osseward and Pfaff, 2019](#); [Osseward et al., 2021](#)). Furthermore, these neurons were most commonly (~80%) contacted by the CST. Our combined stimulation paradigm did not alter the targeting of this specific subpopulation of spinal interneurons. Gait analysis, more specifically fore- and hindlimb coupling, further indicated changes upon coordinated stimulation, in line with the role of long-range projecting spinal V2a neurons ([Dougherty and Kiehn, 2010](#); [Zhong et al., 2010](#); [Ruder et al., 2016](#)). We can however not exclude the possibility that the other non-V2a positive subpopulation, which is also contacted and thus recruited in the detour circuit, plays a significant role in the functional improvements. Interestingly, a recent study unraveled Vsx2 expressing neurons as essential for functional recovery upon lumbar epidural electrical stimulation ([Kathe et al., 2022](#)). These neurons originate from cardinal class V2a neurons, further validating their critical contribution to functional recovery after SCI.

Taken together, our study demonstrates that a refined anatomical understanding of the neuronal circuits that reform in the injured CNS ([Bareyre et al., 2004](#); [Courtine et al., 2008](#); [Ueno et al., 2012](#); [Zörner et al., 2014](#); [Jacobi and Bareyre, 2015](#); [Raineteau and Schwab, 2001](#)) empowers the design of targeted multilevel neurostimulation strategies that selectively foster adaptive circuit rewiring and thereby unlock the CNS's potential for recovery.

Materials and methods

Animals

C57/BL6 and VGlut2-Cre mice (The Jackson Laboratory; Slc17a6tm2(-cre)Lowl/MwarJ, Strain 016963; [Vong et al., 2011](#)) were used (6–12-wk-old). All animal experiments were performed in accordance with the regulations of the animal welfare act and protocols approved by the Regierung von Oberbayern.

Production of AAV vectors

The following plasmids were purchased from Addgene: AAV-hSyn-eGFP (#114213), AAV-hSyn-hM3D(G_q)-mCherry (#50474), AAV-hSyn-DIO-hM3D(G_q)-mCherry (#44361), and pENN-AAV-hSyn-CRE-WPRE.hGH (#105553). AAV8-hSyn-DIO-hM3D(G_q)-eGFP-WPREs was purchased from BrainVTA. To produce viral particles, HEK293T cells were grown in DMEM (low glucose, GlutaMAX) supplemented with 10% fetal bovine serum. Cells were transfected by using polyethylenimine solution with a 1:1:

1 molar ratio of helper, capsid, and desired construct plasmids in RPMI medium without glutamine and serum. 5 h after transfection, the media was changed back to serum-supplemented DMEM and the cells were kept for 3 d before harvesting. The supernatant was harvested 2 and 3 d after transfection and kept at 4°C. The supernatant was centrifuged (4,200 rpm for 10 min) to collect cell debris and then filtered (0.45 micron). For concentration, 15-min centrifugation rounds (4,200 rpm, 4°C) through 100 kD AMICON filters were performed. Titters were determined using qPCR. Viral aliquots were stored at -80°C until used.

Surgical procedures

Mice were orally administered meloxicam (Metacam, 1.5 mg/ml, Boehringer Ingelheim) and anesthetized with intraperitoneal injections of MMF (medetomidin 0.5 mg/kg, Orion Pharma; midazolam 5.0 mg/kg, Ratiopharm; fentanyl 0.05 mg/kg, B. Braun) before surgical procedures. The depth of anesthesia was regularly controlled to ensure there was no reflex retraction from paw pinching. After surgery, mice were injected subcutaneously with an antagonist mixture (atipamezole 2.5 mg/kg, Provident Pharmaceuticals; flumazenil 0.5 mg/kg, Hameln Pharma GmbH; and naloxon 1.2 mg/kg, B. Braun). Prior to and after surgical procedures, mice were kept on a heating pad. Mice received meloxicam (Metacam, 1.5 mg/ml) orally for at least 3 d after the surgery.

Tracing hindlimb CST

The skin was cut and a local anesthetic (Xylocaine 2%, Aspen Pharma) was applied. Bilateral cortical injections of AAV2/8-hSyn-eGFP (titer: 5×10^{12} GC/ml) or AAV2/8-hSyn-hM3D(Gq)-mCherry (titer: 5×10^{12} GC/ml) were used to label/stimulate the hindlimb CST using fine pulled glass micropipettes (coordinates from bregma: -1.3 mm caudal, ± 1.2 mm lateral, and 0.6 mm depth, targeting layer V of the cortex). The wound was closed with skin staples.

Labeling of LPSNs

To express DREADDs in LPSNs, combined bilateral injections of AAV2/8-hSyn-DIO-hM3D(Gq)-mCherry (titer: 2×10^{12} GC/ml) at cervical levels C3–C4 (coordinates from midline: ± 0.3 mm lateral, 0.6 mm depth) and pENN-rAAV-hSyn-CRE-WPRE.hGH (titer: 4×10^{12} GC/ml) at lumbar level L1 (coordinates from midline: ± 0.3 mm lateral, 0.6 mm depth) were used. To fluorescently label LPSNs, combined bilateral injections of rAAV-hSyn-eGFP (titer: 1×10^{12}) at lumbar level L1 coordinates from midline (± 0.3 mm lateral, 0.6 mm depth) were used. The muscles were sutured and the skin was closed with skin staples.

Midthoracic dorsal hemisection

Muscles were ripped to expose the spinal cord after which a local anesthetic was applied (Xylocaine 2%). Fine iridectomy scissors were used to inflict a bilateral transection of the main dorsal and minor dorsolateral CST at thoracic level T8. After hemisection, the muscles were sutured and the skin was closed with skin staples.

Activity modulation using DREADDs

For DREADD-based CST, LPSN, and combined stimulation experiments, the mice were randomized into control and treatment groups at 3 dpi and received subcutaneous injections of either saline or CNO (0.1 mg/kg diluted in saline; #141704; Abcam) until sacrifice.

Tissue processing and immunohistochemistry (IHC)

To prepare tissues for IHC, mice were perfused with PBS-heparin and 4% paraformaldehyde (PFA). Brains and spinal cords were postfixed overnight in 4% PFA and washed with PBS before microdissection. Tissues were transferred to 30% sucrose solution for two nights before freezing in Tissue-Tek OCT. 40- μ m coronal sections were cut and washed three times with PBS before on-slide mounting for IHC. Tissues were blocked with 5% horse serum before application of the following primary antibodies: rat eGFP (1/1,000, #sc-101536; Santa Cruz Biotechnologies), presynaptic marker rabbit Vglut1/2 (1/500, #135 503; Synaptic Systems), goat mCherry (1/1,000, #AB0081-200; Sicgen Antibodies), postsynaptic scaffolding protein guinea pig Homer (1/500, #160 004; Synaptic Systems), guinea pig c-fos (1/250, #226 004; Synaptic Systems), sheep ZFH3 (1/500, #AF7384), and rabbit NFIB (1/250, #NBP1-81000). After overnight incubation of primary antibodies, overnight incubation of the following secondary antibodies followed: anti-rabbit AF647 (1/500, #A32795; Thermo Fisher Scientific), anti-goat AF594 (1/1,000, #A11058; Thermo Fisher Scientific), anti-guinea pig Cy3 1/500, #706-165-148; Jackson ImmunoResearch), anti-guinea pig AF633 (1/500, #SAB4600129; Sigma-Aldrich), and anti-sheep AF647 (#A21448; Thermo Fisher Scientific), all produced in donkeys. Three 10-min PBS wash steps were performed after primary and secondary antibody incubations. To label nuclei or neuronal somata, DAPI (1/10,000) or Neurotrace (1/100) were applied during the final wash steps of the secondary incubations. Slides were mounted with citifluor.

Image acquisition

To visualize and quantify exiting collaterals, an inverted Leica THUNDER imaging system was used fitted with LED fluorescence excitation (475, 555 nm) and an HC PL FLUOTAR 10 \times /0.32 PH1 objective. Emission was collected through a multibandpass filter (519/25 and 594/32 nm) onto a Leica sCMOS DFC9000 GT camera (2,048 \times 2,048 pixels). For synaptic and activity recordings, an inverted Leica SP8X WLL system was used in confocal mode with an HC PL APO 40 \times /1.30 Oil CS2 objective. Excitation was achieved with a pulsed white light laser (470–670 nm) and a continuous wave 405 nm excitation laser. An acousto-optical beam splitter with gated hybrid detectors and PMTs was used for collecting fluorescence emission. For synaptic recordings, the pixel size was adjusted to allow deconvolution. Lesion volumes were recorded on a Leica DM4 widefield system fitted with an HC PL APO 10 \times /0.45 objective.

Image processing

For quantification of c-fos expression, Imaris was used to automatically detect neuronal DAPI nuclei based on hM3D(Gq)-mCherry expression. The mean intensity of c-fos expression

inside nuclei was quantified. For the quantification of exiting collaterals, the number of exiting collaterals was normalized to the main CST labeling density. For synaptic quantification, confocal recordings were first deconvolved using a theoretical point spread function based on the optical properties of the imaging system using Huygens (SVI). Then, automatic detection of boutons along collaterals was used (spot detection feature with region growing algorithm, Imaris) with a fixed defined threshold for presynaptic and postsynaptic staining intensity per experiment. For contacts onto LPSNs or Neurotrace-labeled cells, their surfaces were rendered and CST boutons touching either of the surfaces, using the shortest distance parameter, were counted.

Behavior: Ladder rung and kinematics

Mice were habituated three times on a horizontal ladder rung with irregularly spaced ladders and the treadmill (speed of 10 and 20 cm/s). Baseline recordings were performed the day before dorsal hemisection with the following recordings at 3 and 21 dpi. A GoPro 8 camera (120 fps) was used to record either three full runs or 1-min recordings for ladder rung and kinematics recordings, respectively. Parameters used for feature labeling and model training in DeepLabCut were identical to previously published work (Aljovic et al., 2022; Mathis et al., 2018). The ALMA toolbox (Aljovic et al., 2022) was used for the validation of detected foot faults and extraction of kinematic parameters.

Behavior: Catwalk XT

To assess gait, we used Catwalk XT (Hamers et al., 2006). All animals were habituated three times before baseline recording. Three valid runs were recorded for each time point (preinjury, 3 dpi, and 21 dpi). A run was included when the preset requirements of the system were fulfilled: a minimum run duration of 0.5 s, a maximum run duration of 4 s, and a maximum speed variation of 60%, to ensure that the animal walked on the runway without interruptions.

Behavior: In cage

To evaluate the number of scratching and grooming events 30 min, 24, and 48 h after CNO injections, mice were recorded in their cage with a GoPro 8 camera. Boris was used as a logging software to detect and quantify scratching and grooming events.

Electromyography (EMG) recordings

Animals were anesthetized with an intraperitoneal injection of ketamine/xylazine (ketamine, 87 mg/kg; xylazine, 13 mg/kg) and then supplemented with subdermal injections of ketamine alone (33 mg/kg) as needed by assessment of the breathing rate and hindpaw pinch response. A hole was made at the coordinates -1.3 mm posterior to bregma, 1 mm lateral to bregma, and over the sensorimotor cortex of the right hemisphere. The dura was removed and the exposed brain was kept moist with saline. EMG recordings were performed as previously described (Bareyre et al., 2004; Lang et al., 2013). Unipolar stimulation of the right motor cortex was performed using parylene-insulated tungsten microelectrodes of 1 M Ω impedance (TM33B10, WPI). A chlorinated silver wire was placed in contact with the brain at

the anterior-lateral edge of the craniotomy and served as the return electrode. Differential EMG recording in the ipsilateral hindlimb was performed using subdermal needle electrodes (TerniMed) in a bipolar configuration. The electrodes were inserted into the hindlimb Biceps femoris muscle group. The hindlimb was then placed in an elevated position on foam pads to assist visualization of muscle movements and to maintain the correct placement of the needle electrodes. Signals were amplified (1 k), band-pass filtered (low 10 Hz, high 5 kHz, A-M Systems Model 1800), digitized using a Micro 1,401 data acquisition unit (CED Ltd; Cambridge Electronic Design), and then sent to a computer running Spike2 software (Cambridge Electronic Design).

EMG stimulation protocol and analysis

The stimulations were performed in the middle of the hindlimb motor cortex region. If necessary, slight adjustments in the mediolateral direction were made to prevent the electrode from penetrating blood vessels. Monophasic cathodal pulses (10-ms train duration at 300 Hz, 0.2-ms pulse duration) were applied through the electrode at an interval of 1 s using an iso-flex stimulus isolator triggered by a Master 8 stimulator (both from A.M.P.I. Instruments). The electrode was lowered vertically into the cortex initially using a high stimulus current (60–100 μ A) until movement of the contralateral hindlimb was detected (10 trials per site). Hindlimb activation was classified as a movement of the digits, the distal or proximal joints, and/or muscle twitch. To determine the threshold of ipsilateral hindlimb activation, the depth of the electrode was first optimized to give maximal contralateral hindlimb movement. At this point, the current was reduced to zero, and then increased in increments of 10 μ A until the EMG signal in the ipsilateral hindlimb appeared. If no EMG signal was detected at 200 μ A the site was deemed unresponsive. In situations where no response was evident, it was confirmed that the needle electrodes were correctly positioned and functional by squeezing the ipsilateral paw. Using Spike2 software, latencies were also determined and measured to the onset of the EMG response, as well as the activation duration, maximum amplitude, and root-mean-square amplitude on three consecutive EMG signals recorded at the same stimulation site.

RNA sequencing

Manual perfusion with ice-cold PBS was performed 21 dpi. Cervical level C3–C4 of the spinal cord was removed and snap-frozen in liquid nitrogen. For RNA isolation, the RNeasy Lipid Tissue Mini Kit (Qiagen) was used according to the manufacturer's protocol. RNA samples were then processed for sequencing using the Colibri 3' mRNA library preparation kit for Illumina systems. Before sending for sequencing, the quality of the library was assessed on a Bioanalyzer using DNA 1000 Chips (both from Agilent Technologies). Samples are sequenced by Laboratory for Functional Genome Analysis (LAFUGA) for single-end 50 bp on a HiSeq 1,500. All RNASeq analysis is performed using Galaxy platform (Jalili et al., 2020). In brief, Fastq files were analyzed using FastQC52 for quality control. Reads were aligned to GRCm38 mouse genome using Star aligner

(Dobin et al., 2013). Read counts and differential gene expression analysis were performed using DESeq2 (Anders et al., 2015). Single genes were annotated using Annotate DESeq2 (Love et al., 2014) available at <https://galaxyproject.org/eu/>. PCA visualization was generated using DESeq2. Statistically significant differentially expressed genes were defined using a cutoff of adjusted $P < 0.05$ and $\log_2(\text{fold-change})$. Pathway analysis was obtained using gProfiler (Reimand et al., 2007). In brief, the top 100 differentially expressed genes were used to find the most significant cellular pathways. Genes were arranged by order of statistical significance. The data has been deposited on Figshare (<https://doi.org/10.6084/m9.figshare.21679415.v1>; Steenbergen et al., 2022).

Statistical analysis

Prism software (GraphPad, version 9) was used for statistical analysis. All datasets were tested for normality using the Shapiro-Wilk test. Parametric and non-parametric tests used are indicated in the figure legends. All results are represented as mean \pm SEM. In all analyses, $P < 0.05$ was considered statistically significant and all significance levels are indicated in the figure legends as follows: *, $P < 0.05$; **, $P < 0.01$; ***, $P < 0.001$.

Online supplemental material

Fig. S1 shows that repetitive CNO injections do not lead to increased activity in the brain or spinal cord in the absence of DREADDs. In Fig. S2, we show that sprouting of the CST is not altered upon distinct stimulation paradigms, we provide evidence of equal viral labeling amongst groups, and we indicate that presynaptic maturation is enhanced while homer expression remains unaltered. Fig. S3 displays a heatmap of the top 100 altered genes upon coordinated stimulation of the CST and LPSNs. Fig. S4 contains controls for CNO-induced behavioral effects (i) in the absence of DREADDs, (ii) in the presence of DREADDs in uninjured animals, and (iii) at pretreatment time points in our experimental paradigms. In Fig. S5, we display heatmaps of the PC1 and PC2 loadings for kinematics parameters for the spinal and coordinated stimulation paradigms together with the heatmaps for PC1 and PC2 loadings of the CatWalk analysis.

Data availability

All data are available in the manuscript or the supplementary materials. Raw data are available upon reasonable request to the corresponding authors.

Acknowledgments

The authors thank the SyNergy Mesoscale Hub, J. Schmitt, and K. Plesniar for AAV production. We also thank the Core Facility Bioimaging of the Biomedical Center for using the widefield and confocal imaging systems. We thank the Laboratory for Functional Genome Analysis (LAFUGA) for RNA sequencing. We thank Martin Kerschensteiner for critically reading the manuscript.

Work in F.M. Bareyre's lab is supported by grants from the Deutsche Forschungsgemeinschaft (DFG, SFB 870 Project ID

118803580, TRR274 Project ID 408885537) and by the Munich Center for Systems Neurology (DFG, SyNergy; EXC 2145/ID 390857198). This project was also supported by the Institute for Research on Paraplegia (IRP). V. Van Steenbergen is supported by a post-doctoral fellowship from the Humboldt Foundation. J. Fourneau is supported by a post-doctoral fellowship from the Wings for Life foundation.

Author contributions: V. Van Steenbergen: Conceptualization, methodology, validation, formal analysis, investigation, writing—original draft, writing—review and editing, visualization, supervision, funding acquisition. L. Burattini: Validation, formal analysis, investigation, writing—review and editing. M. Trumpp: Validation, formal analysis, investigation, writing—review and editing. J. Fourneau: Methodology, validation, formal analysis, investigation, writing—review and editing, funding acquisition. A. Aljović: Methodology, data curation, validation, formal analysis, investigation, writing—review and editing. M. Chahin: Validation, formal analysis, investigation, writing—review and editing. H. Oh: Validation, formal analysis, investigation, writing—review and editing. M. D'Ambra: Validation, formal analysis, investigation, writing—review and editing. F.M. Bareyre: Conceptualization, methodology, validation, resources, writing—original draft, writing—review and editing, visualization, supervision, project administration, funding acquisition.

Disclosures: The authors declare no competing interests exist.

Submitted: 8 April 2022

Revised: 26 October 2022

Accepted: 15 December 2022

References

- Alexander, G.M., S.C. Rogan, A.I. Abbas, B.N. Armbruster, Y. Pei, J.A. Allen, R.J. Nonneman, J. Hartmann, S.S. Moy, M.A. Nicolelis, et al. 2009. Remote control of neuronal activity in transgenic mice expressing evolved G protein-coupled receptors. *Neuron*. 63:27–39. <https://doi.org/10.1016/j.neuron.2009.06.014>
- Aljovic, A., S. Zhao, M. Chahin, C. de la Rosa, V. Van Steenbergen, M. Kerschensteiner, and F.M. Bareyre. 2022. A deep learning-based toolbox for automated limb motion analysis (ALMA) in murine models of neurological disorders. *Commun. Biol.* 5:131. <https://doi.org/10.1038/s42003-022-03077-6>
- Osseward, P.J., II, N.D. Amin, J.D. Moore, B.A. Temple, B.K. Barriga, L.C. Bachmann, F. Beltran Jr, M. Gullo, R.C. Clark, S.P. Driscoll, et al. 2021. Conserved genetic signatures parcellate cardinal spinal neuron classes into local and projection subsets. *Science*. 372:385–393. <https://doi.org/10.1126/science.abe0690>
- Anders, S., P.T. Pyl, and W. Huber. 2015. HTSeq: A Python framework to work with high-throughput sequencing data. *Bioinformatics*. 31:166–169. <https://doi.org/10.1093/bioinformatics/btu638>
- Angeli, C.A., M. Boakye, R.A. Morton, J. Vogt, K. Benton, Y. Chen, C.K. Ferreira, and S.J. Harkema. 2018. Recovery of over-ground walking after chronic motor complete spinal cord injury. *N. Engl. J. Med.* 379: 1244–1250. <https://doi.org/10.1056/NEJMoa1803588>
- Bachmann, L.C., A. Matis, N.T. Lindau, P. Felder, M. Gullo, and M.E. Schwab. 2013. Deep brain stimulation of the midbrain locomotor region improves paretic hindlimb function after spinal cord injury in rats. *Sci. Transl. Med.* 5:208ra146. <https://doi.org/10.1126/scitranslmed.3005972>
- Bareyre, F.M., M. Kerschensteiner, O. Raineteau, T.C. Mettenleiter, O. Weinmann, and M.E. Schwab. 2004. The injured spinal cord spontaneously forms a new intraspinal circuit in adult rats. *Nat. Neurosci.* 7: 269–277. <https://doi.org/10.1038/nn1195>

- Bonizzato, M., N.D. James, G. Pidpruzhnykova, N. Pavlova, P. Shkorbatova, L. Baud, C. Martinez-Gonzalez, J.W. Squair, J. DiGiovanna, Q. Barraud, et al. 2021. Multi-pronged neuromodulation intervention engages the residual motor circuitry to facilitate walking in a rat model of spinal cord injury. *Nat. Commun.* 12:1925. <https://doi.org/10.1038/s41467-021-22137-9>
- Botterill, J.J., K.Y. Vinod, K.J. Gerencer, C.M. Teixeira, J.J. LaFrancois, and H.E. Scharfman. 2021. Bidirectional regulation of cognitive and anxiety-like behaviors by dentate gyrus mossy cells in male and female mice. *J. Neurosci.* 41:2475–2495. <https://doi.org/10.1523/JNEUROSCI.1724-20.2021>
- Bradley, P.M., C.K. Denecke, A. Aljovic, A. Schmalz, M. Kerschensteiner, and F.M. Bareyre. 2019. Corticospinal circuit remodeling after central nervous system injury is dependent on neuronal activity. *J. Exp. Med.* 216: 2503–2514. <https://doi.org/10.1084/jem.20181406>
- Brommer, B., M. He, Z. Zhang, Z. Yang, J.C. Page, J. Su, Y. Zhang, J. Zhu, E. Gouy, J. Tang, et al. 2021. Improving hindlimb locomotor function by Non-invasive AAV-mediated manipulations of propriospinal neurons in mice with complete spinal cord injury. *Nat. Commun.* 12:781. <https://doi.org/10.1038/s41467-021-20980-4>
- Bullitt, E. 1990. Expression of c-fos-like protein as a marker for neuronal activity following noxious stimulation in the rat. *J. Comp. Neurol.* 296: 517–530. <https://doi.org/10.1002/cne.902960402>
- Carmel, J.B., and J.H. Martin. 2014. Motor cortex electrical stimulation augments sprouting of the corticospinal tract and promotes recovery of motor function. *Front. Integr. Neurosci.* 8:51. <https://doi.org/10.3389/fnint.2014.00051>
- Carmel, J.B., H. Kimura, L.J. Berrol, and J.H. Martin. 2013. Motor cortex electrical stimulation promotes axon outgrowth to brain stem and spinal targets that control the forelimb impaired by unilateral corticospinal injury. *Eur. J. Neurosci.* 37:1090–1102. <https://doi.org/10.1111/ejn.12119>
- Carmel, J.B., H. Kimura, and J.H. Martin. 2014. Electrical stimulation of motor cortex in the uninjured hemisphere after chronic unilateral injury promotes recovery of skilled locomotion through ipsilateral control. *J. Neurosci.* 34:462–466. <https://doi.org/10.1523/JNEUROSCI.3315-13.2014>
- Chen, B., Y. Li, B. Yu, Z. Zhang, B. Brommer, P.R. Williams, Y. Liu, S.V. Hegarty, S. Zhou, J. Zhu, et al. 2018. Reactivation of dormant relay pathways in injured spinal cord by KCC2 manipulations. *Cell.* 174: 521–535.e13. <https://doi.org/10.1016/j.cell.2018.06.005>
- Courtine, G., B. Song, R.R. Roy, H. Zhong, J.E. Herrmann, Y. Ao, J. Qi, V.R. Edgerton, and M.V. Sofroniew. 2008. Recovery of supraspinal control of stepping via indirect propriospinal relay connections after spinal cord injury. *Nat. Med.* 14:69–74. <https://doi.org/10.1038/nm1682>
- Deng, W.W., G.Y. Wu, L.X. Min, Z. Feng, H. Chen, M.L. Tan, J.F. Sui, H.L. Liu, and J.M. Hou. 2021. Optogenetic neuronal stimulation promotes functional recovery after spinal cord injury. *Front. Neurosci.* 15:640255. <https://doi.org/10.3389/fnins.2021.640255>
- Dobin, A., C.A. Davis, F. Schlesinger, J. Drenkow, C. Zaleski, S. Jha, P. Batut, M. Chaisson, and T.R. Gingeras. 2013. STAR: Ultrafast universal RNA-seq aligner. *Bioinformatics.* 29:15–21. <https://doi.org/10.1093/bioinformatics/bts635>
- Dougherty, K.J., and O. Kiehn. 2010. Functional organization of V2a-related locomotor circuits in the rodent spinal cord. *Ann. N.Y. Acad. Sci.* 1198: 85–93. <https://doi.org/10.1111/j.1749-6632.2010.05502.x>
- Dragunow, M., and R. Faull. 1989. The use of c-fos as a metabolic marker in neuronal pathway tracing. *J. Neurosci. Methods.* 29:261–265. [https://doi.org/10.1016/0165-0270\(89\)90150-7](https://doi.org/10.1016/0165-0270(89)90150-7)
- Granier, C., J. Schwarting, E. Fourli, F. Laage-Gaupp, A.A. Hennrich, A. Schmalz, A. Jacobi, M. Wesolowski, K.K. Conzelmann, and F.M. Bareyre. 2020. Formation of somatosensory detour circuits mediates functional recovery following dorsal column injury. *Sci. Rep.* 10:10953. <https://doi.org/10.1038/s41598-020-67866-x>
- Hamers, F.P., G.C. Koopmans, and E.A. Joosten. 2006. CatWalk-assisted gait analysis in the assessment of spinal cord injury. *J. Neurotrauma.* 23: 537–548. <https://doi.org/10.1089/neu.2006.23.537>
- Hilton, B.J., E. Anenberg, T.C. Harrison, J.D. Boyd, T.H. Murphy, and W. Tetzlaff. 2016. Re-establishment of cortical motor output maps and spontaneous functional recovery via spared dorsolaterally projecting corticospinal neurons after dorsal column spinal cord injury in adult mice. *J. Neurosci.* 36:4080–4092. <https://doi.org/10.1523/JNEUROSCI.3386-15.2016>
- Hilton, B.J., A. Husch, B. Schaffran, T.C. Lin, E.R. Burnside, S. Dupraz, M. Schelski, J. Kim, J.A. Müller, S. Schoch, et al. 2022. An active vesicle priming machinery suppresses axon regeneration upon adult CNS injury. *Neuron.* 110:51–69.e7. <https://doi.org/10.1016/j.neuron.2021.10.007>
- Jacobi, A., and F.M. Bareyre. 2015. Regulation of axonal remodeling following spinal cord injury. *Neural Regen. Res.* 10:1555–1557. <https://doi.org/10.4103/1673-5374.167748>
- Jacobi, A., K. Loy, A.M. Schmalz, M. Hellsten, H. Umemori, M. Kerschensteiner, and F.M. Bareyre. 2015. FGF22 signaling regulates synapse formation during post-injury remodeling of the spinal cord. *EMBO J.* 34: 1231–1243. <https://doi.org/10.15252/embj.201490578>
- Jalili, V., E. Afgan, Q. Gu, D. Clements, D. Blankenberg, J. Goecks, J. Taylor, and A. Nekrutenko. 2020. The Galaxy platform for accessible, reproducible and collaborative biomedical analyses: 2020 update. *Nucleic Acids Res.* 48:W395–W402. <https://doi.org/10.1093/nar/gkaa434>
- Kathe, C., M.A. Skinnider, T.H. Hutson, N. Regazzi, M. Gautier, R. Demesmaeker, S. Komi, S. Ceto, N.D. James, N. Cho, et al. 2022. The neurons that restore walking after paralysis. *Nature.* 611:540–547. <https://doi.org/10.1038/s41586-022-05385-7>
- Lang, C., X. Guo, M. Kerschensteiner, and F.M. Bareyre. 2012. Single collateral reconstructions reveal distinct phases of corticospinal remodeling after spinal cord injury. *PLoS One.* 7:e30461. <https://doi.org/10.1371/journal.pone.0030461>
- Lang, C., P.M. Bradley, A. Jacobi, M. Kerschensteiner, and F.M. Bareyre. 2013. STAT3 promotes corticospinal remodelling and functional recovery after spinal cord injury. *EMBO Rep.* 14:931–937. <https://doi.org/10.1038/embor.2013.117>
- Liebetanz, D., and D. Merkle. 2006. Effects of commissural de- and myelination on motor skill behaviour in the cuprizone mouse model of multiple sclerosis. *Exp. Neurol.* 202:217–224. <https://doi.org/10.1016/j.expneurol.2006.05.032>
- Love, M.I., W. Huber, and S. Anders. 2014. Moderated estimation of fold change and dispersion for RNA-seq data with DESeq2. *Genome Biol.* 15: 550. <https://doi.org/10.1186/s13059-014-0550-8>
- Loy, K., and F.M. Bareyre. 2019. Rehabilitation following spinal cord injury: How animal models can help our understanding of exercise-induced neuroplasticity. *Neural Regen. Res.* 14:405–412. <https://doi.org/10.4103/1673-5374.245951>
- Mathis, A., P. Mamidanna, K.M. Cury, T. Abe, V.N. Murthy, M.W. Mathis, and M. Bethge. 2018. DeepLabCut: Markerless pose estimation of user-defined body parts with deep learning. *Nat. Neurosci.* 21:1281–1289. <https://doi.org/10.1038/s41593-018-0209-y>
- Osseward, P.J., II, and S.L. Pfaff. 2019. Cell type and circuit modules in the spinal cord. *Curr. Opin. Neurobiol.* 56:175–184. <https://doi.org/10.1016/j.conb.2019.03.003>
- Pohjonen, M., S. Savolainen, J. Arokoski, and A. Shulga. 2021. Omitting TMS component from paired associative stimulation with high-frequency PNS: A case series of tetraplegic patients. *Clin. Neurophysiol. Pract.* 6: 81–87. <https://doi.org/10.1016/j.cnp.2021.01.004>
- Pulverenti, T.S., M. Zaaya, M. Grabowski, E. Grabowski, M.A. Islam, J. Li, L.M. Murray, and M. Knikou. 2021. Neurophysiological changes after paired brain and spinal cord stimulation coupled with locomotor training in human spinal cord injury. *Front. Neurol.* 12:627975. <https://doi.org/10.3389/fneur.2021.627975>
- Raineteau, O., and M.E. Schwab. 2001. Plasticity of motor systems after incomplete spinal cord injury. *Nat. Rev. Neurosci.* 2:263–273. <https://doi.org/10.1038/35067570>
- Reimand, J., M. Kull, H. Peterson, J. Hansen and J. Vilo. 2007. g:Profiler: A web-based toolset for functional profiling of gene lists from large-scale experiments. *Nucleic Acids Res.* 35:W193–W200. <https://doi.org/10.1093/nar/gkm226>
- Roth, B.L. 2016. DREADDs for neuroscientists. *Neuron.* 89:683–694. <https://doi.org/10.1016/j.neuron.2016.01.040>
- Ruder, L., A. Takeoka, and S. Arber. 2016. Long-distance descending spinal neurons ensure quadrupedal locomotor stability. *Neuron.* 92:1063–1078. <https://doi.org/10.1016/j.neuron.2016.10.032>
- Shulga, A., P. Lioumis, E. Kirveskari, S. Savolainen, and J.P. Mäkelä. 2021. A novel paired associative stimulation protocol with a high-frequency peripheral component: A review on results in spinal cord injury rehabilitation. *Eur. J. Neurosci.* 53:3242–3257. <https://doi.org/10.1111/ejn.15191>
- Steenbergen, V., L. Burattini, M. Trumpp, J. Fourneau, A. Aljovic, M. Chahin and B. Florence. 2022. Coordinated supraspinal and spinal neurostimulation guides circuit rewiring and unlocks motor recovery after spinal cord injury (RNASeq Data). *Figshare.* <https://doi.org/10.6084/m9.figshare.21679415.v1>

- Ueno, M., Y. Hayano, H. Nakagawa, and T. Yamashita. 2012. Intraspinal re-wiring of the corticospinal tract requires target-derived brain-derived neurotrophic factor and compensates lost function after brain injury. *Brain*. 135:1253–1267. <https://doi.org/10.1093/brain/aws053>
- Vaalto, S., A.L. Nyman, and A. Shulga. 2021. Analgesic effect of paired associative stimulation in a tetraplegic patient with severe drug-resistant neuropathic pain: A case report. *Scand. J. Pain*. 21:831–838. <https://doi.org/10.1515/sjpain-2021-0012>
- van den Brand, R., J. Heutschi, Q. Barraud, J. DiGiovanna, K. Bartholdi, M. Huerlimann, L. Friedli, I. Vollenweider, E.M. Moraud, S. Duis, et al. 2012. Restoring voluntary control of locomotion after paralyzing spinal cord injury. *Science*. 336:1182–1185. <https://doi.org/10.1126/science.1217416>
- Van Steenbergen, V., and F.M. Bareyre. 2021. Chemogenetic approaches to unravel circuit wiring and related behavior after spinal cord injury. *Exp. Neurol*. 345:113839. <https://doi.org/10.1016/j.expneurol.2021.113839>
- Vong, L., C. Ye, Z. Yang, B. Choi, S. Chua Jr, and B.B. Lowell. 2011. Leptin action on GABAergic neurons prevents obesity and reduces inhibitory tone to POMC neurons. *Neuron*. 71:142–154. <https://doi.org/10.1016/j.neuron.2011.05.028>
- Wagner, F.B., J.B. Mignardot, C.G. Le Goff-Mignardot, R. Demesmaeker, S. Komi, M. Capogrosso, A. Rowald, I. Seáñez, M. Caban, E. Pirondini, et al. 2018. Targeted neurotechnology restores walking in humans with spinal cord injury. *Nature*. 563:65–71. <https://doi.org/10.1038/s41586-018-0649-2>
- Zhong, G., S. Droho, S.A. Crone, S. Dietz, A.C. Kwan, W.W. Webb, K. Sharma, and R.M. Harris-Warrick. 2010. Electrophysiological characterization of V2a interneurons and their locomotor-related activity in the neonatal mouse spinal cord. *J. Neurosci*. 30:170–182. <https://doi.org/10.1523/JNEUROSCI.4849-09.2010>
- Zörner, B., L.C. Bachmann, L. Filli, S. Kapitza, M. Gullo, M. Bolliger, M.L. Starkey, M. Röthlisberger, R.R. Gonzenbach, and M.E. Schwab. 2014. Chasing central nervous system plasticity: The brainstem's contribution to locomotor recovery in rats with spinal cord injury. *Brain*. 137: 1716–1732. <https://doi.org/10.1093/brain/awu078>

Supplemental material

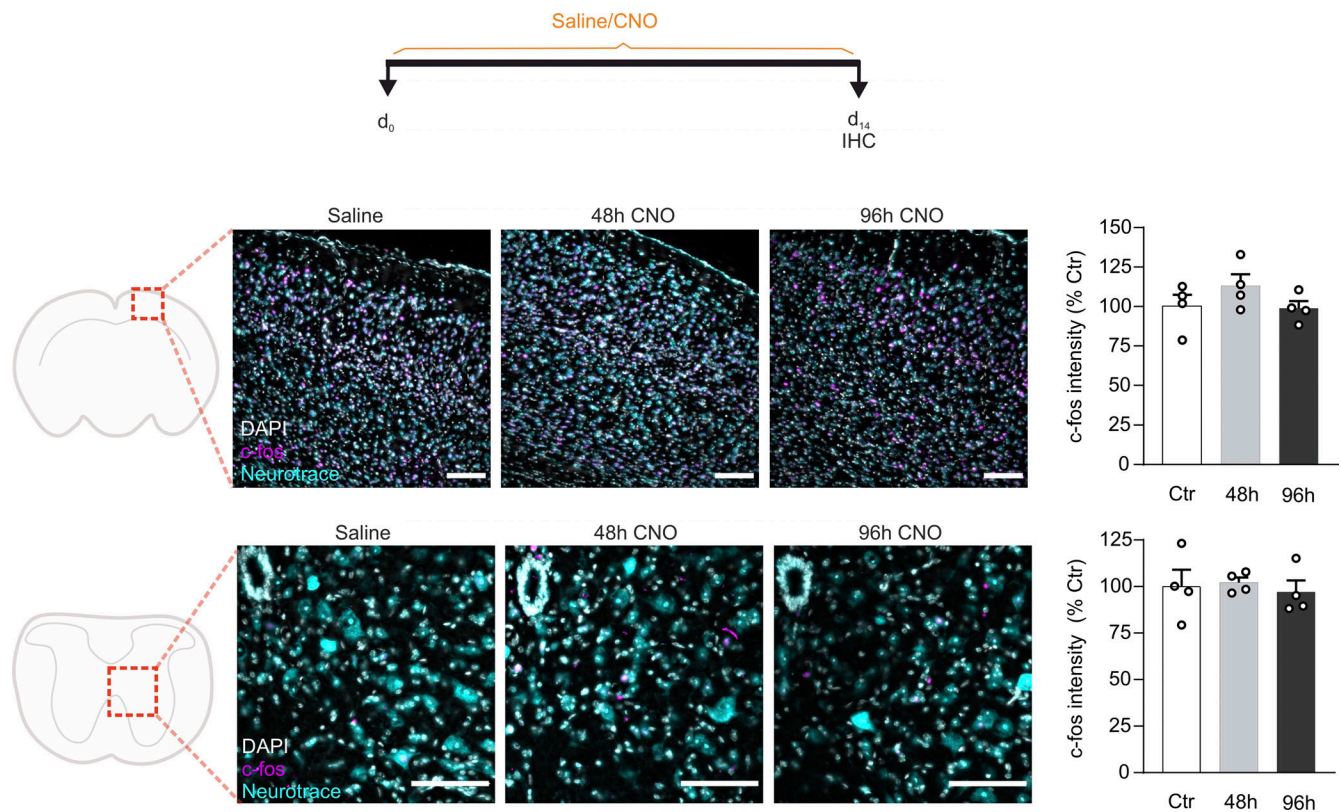


Figure S1. **Repetitive CNO injections do not alter c-fos expression in the absence of activating DREADDs.** Mice were injected with saline (control) or CNO (every 48 or 96 h) for two consecutive weeks and perfused 90 min after the final injection. Brain and spinal cord tissue stained for c-fos and intensity quantification in the hindlimb cortex ($n = 4$ mice) and the ventral area of cervical level C3–C4 ($n = 4$ mice). Scale bars, 100 μ m. Data are represented with the individual biological replicates; the mean and error bars represent the SEM.

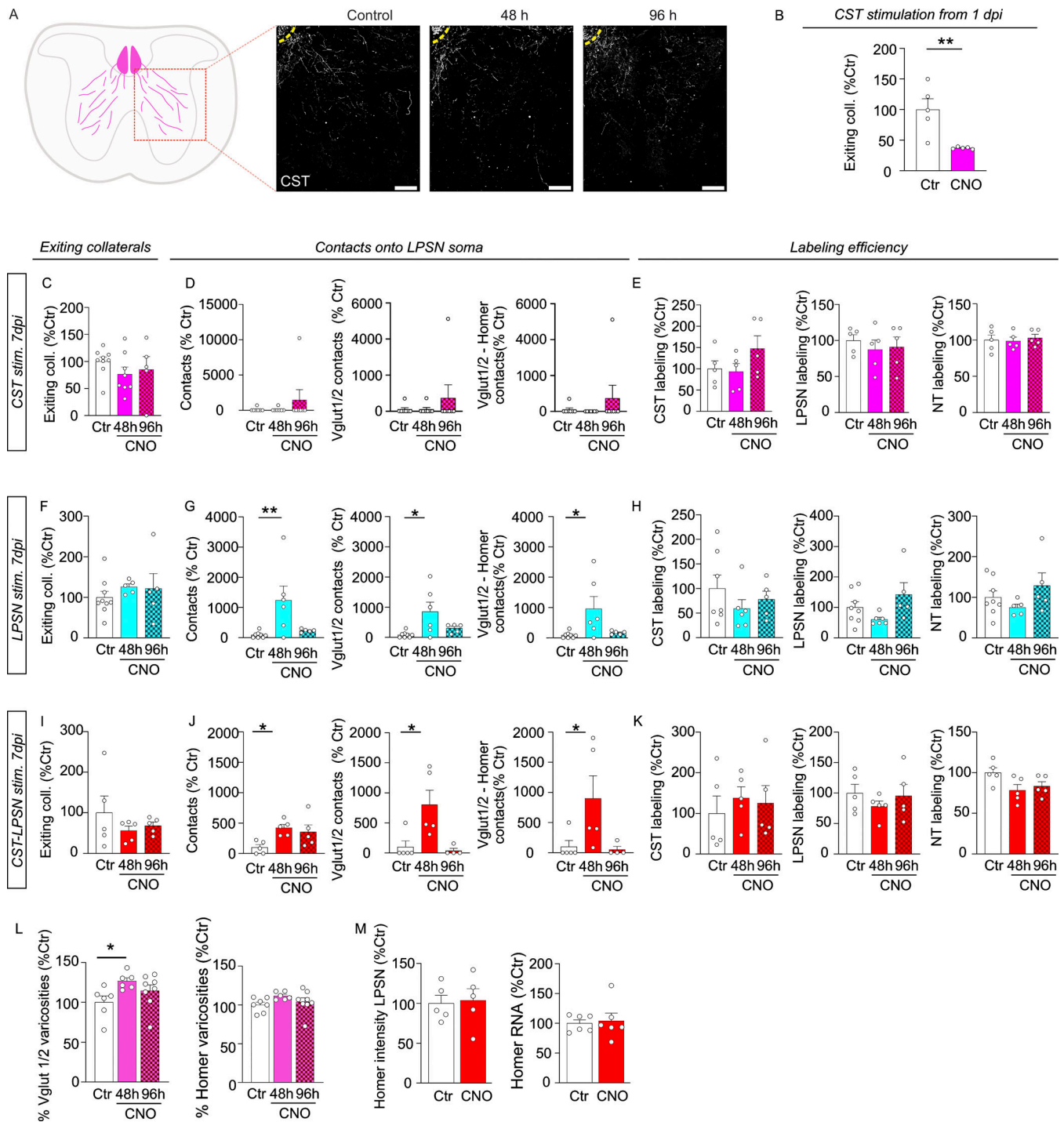


Figure S2. **CST collateral formation is not affected by distinct stimulation protocols, while CST stimulation increases pre- but not postsynaptic maturation.** (A) Overview of exiting collaterals at cervical level C3–C4. (B) Quantification of exiting collaterals upon CST stimulation from 1 dpi every 48 h ($n = 5$ mice). (C) Exiting collateral density at cervical level C3–C4 upon CST stimulation from 7 dpi ($n = 5$ –9 mice). (D) Quantification of CST contacts onto LPSN soma, Vglut1/2-positive contacts, and Vglut1/2-Homer-positive contacts ($n = 5$ mice). (E) Exiting collateral density at cervical level C3–C4 upon LPSN stimulation from 7 dpi ($n = 5$ mice). (F) Quantification of CST contacts onto LPSN soma, Vglut1/2-positive contacts, and Vglut1/2-Homer-positive contacts ($n = 5$ mice). (G) No change in viral labeling or neuronal staining efficiency between all treatment groups was detected for hindlimb CST injections ($n = 5$ mice), retrograde LPSN labeling ($n = 5$ mice; Dunnett's multiple comparisons test), or neurotrace stained area ($n = 5$ mice). (I) Exiting collateral density at cervical level C3–C4 after combined CST and LPSN stimulation from 7 dpi ($n = 5$ mice). (J) Quantification of CST contacts onto LPSN soma, Vglut1/2-positive contacts, and Vglut1/2-Homer-positive contacts ($n = 5$ mice). (K) No change in viral or IHC labeling between all treatment groups was detected for hindlimb CST injections ($n = 5$ mice), LPSN labeling ($n = 5$ mice), or neurotrace stained area ($n = 5$ mice). (L) Maturation of varicosities evaluated as the percentage of Vglut1/2 and Homer-positive boutons following chemogenetic corticospinal stimulation ($n = 5$ mice). (M) Quantification of Homer expression at the protein level in LPSNs ($n = 5$ mice) and Homer mRNA expression in the cervical spinal cord ($n = 6$ mice). Scale bars, 100 μ m. Data are represented with the individual biological replicates, the mean and error bars represent the SEM. *, $P < 0.05$; **, $P < 0.01$; ***, $P < 0.001$.

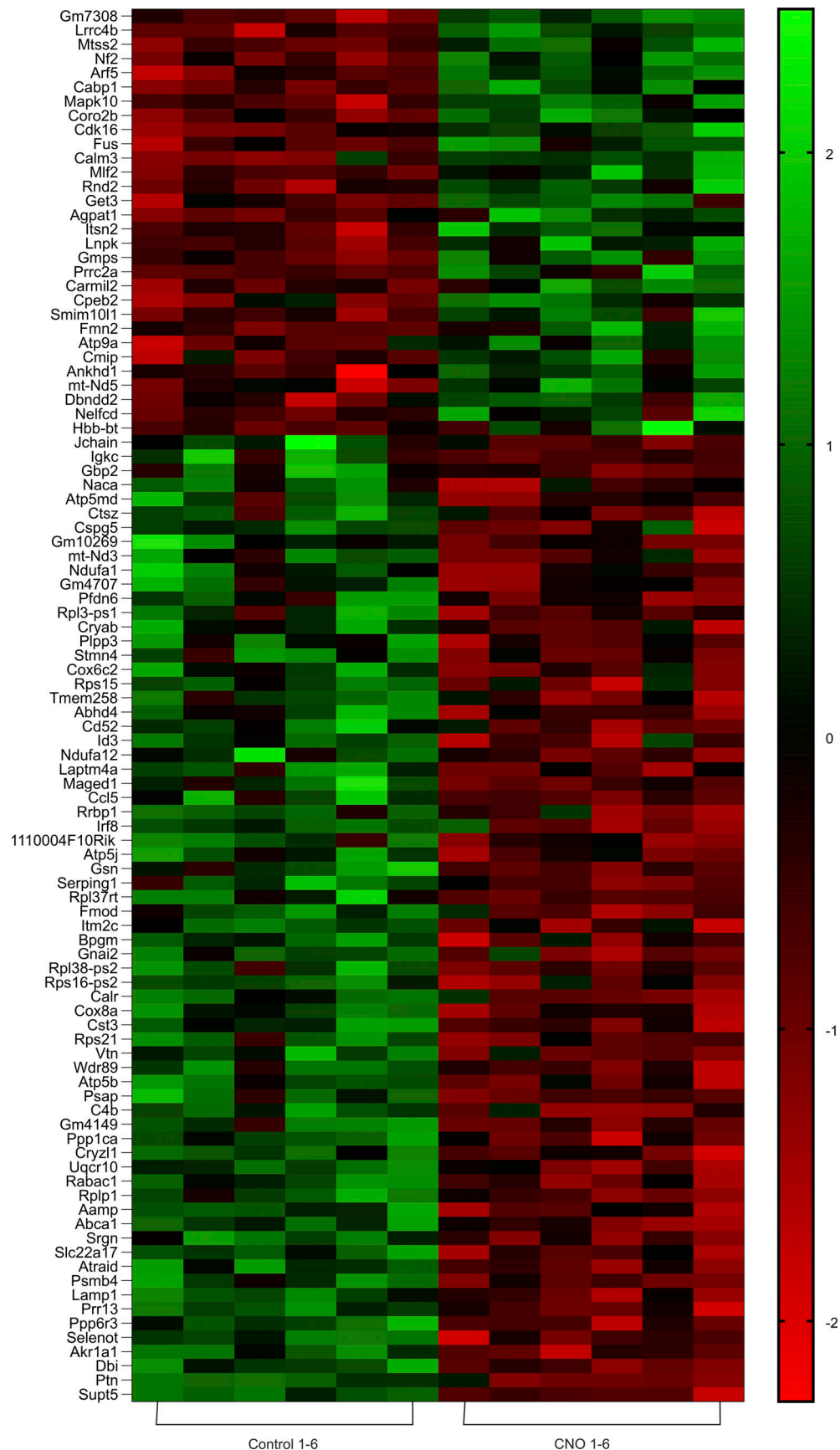


Figure S3. **Transcriptomic changes upon combined CST and LPSN chemogenetic activation after SCI.** Heatmap representing the 98 differentially expressed genes used for GO classification analysis between control and combined stimulation samples ($n = 6$ mice).

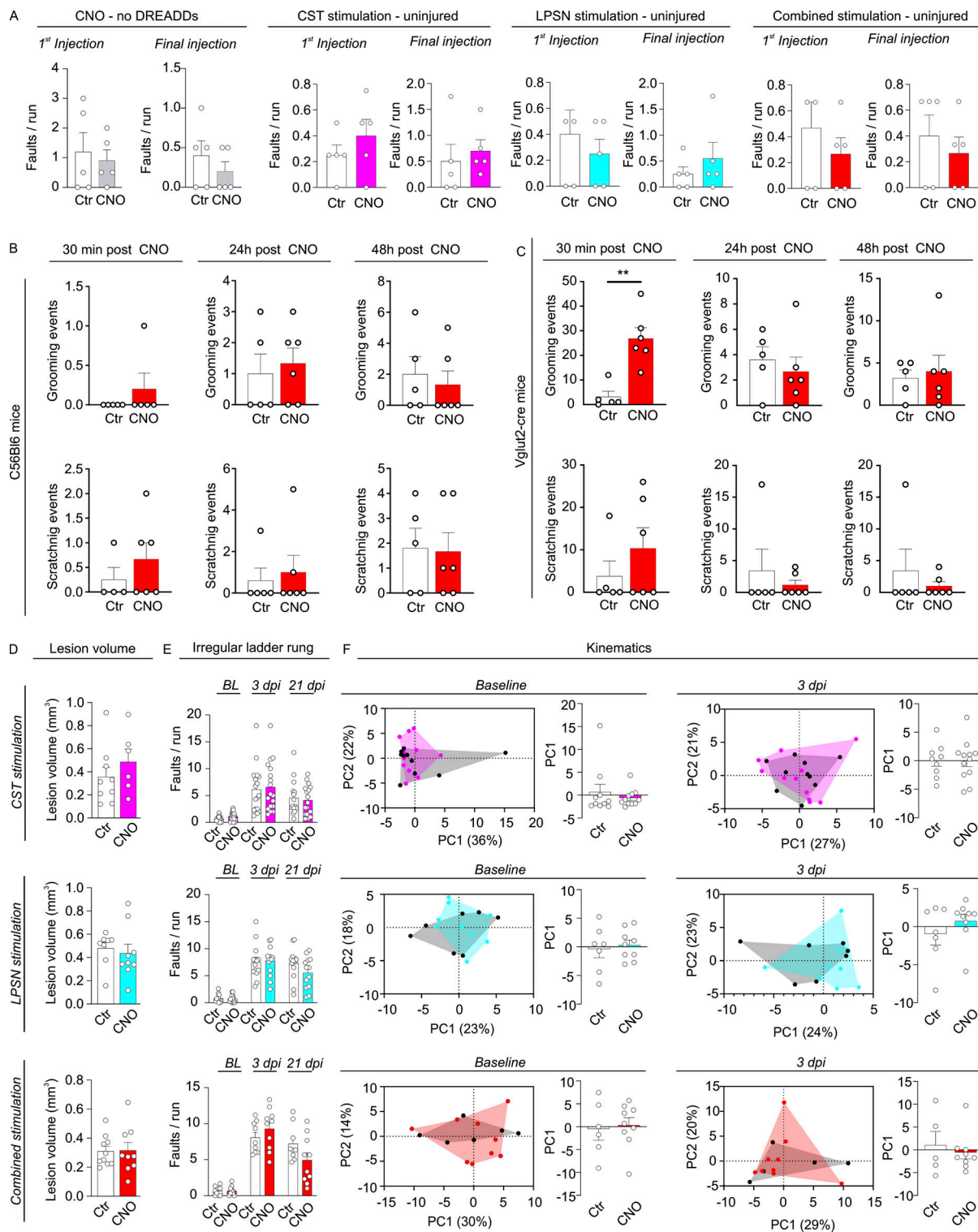


Figure S4. Controlling for behavioral outcomes not related to circuit rewiring. (A) Repetitive administration of saline and CNO (0.1 mg/kg) 30 min after the first or final injection in the absence of DREADDs, upon stimulation of the hindlimb CST, stimulation of LPSNs, or stimulation of the hindlimb CST and LPSNs ($n = 5$ mice). (B and C) In-cage behavior (grooming and scratching events) 30 min, 24, and 48 h after stimulation of corticospinal neurons and LPSNs in C56Bl6 mice and in (C) cervical excitatory neurons in Vglut2Cre mice. (D) Quantification of the lesion volumes for CST ($n = 6-9$ mice), LPSN ($n = 8-9$ mice), and combined CST-LPSN ($n = 9-10$ mice) stimulation. Comparing lesion volumes amongst treatment groups furthermore showed no difference ($n = 6-10$ mice). (E) Quantification of the number of faults on an irregular ladder rung at baseline (before injury) and 3 dpi timepoints before stimulation for CST ($n = 16-18$ mice), LPSN ($n = 13-15$ mice) and combined CST-LPSN ($n = 10$ mice) stimulation paradigms. Comparing the number of faults amongst treatment groups showed no difference at baseline ($n = 10-18$ mice) or 3 dpi ($n = 10-18$ mice). (F) PCA analysis of kinematic parameters between control and treatment groups at baseline and 3 dpi for CST stimulation ($n = 16-18$ mice), LPSN stimulation ($n = 7-9$ mice), and combined stimulation ($n = 5-9$ mice). Data are represented with the individual biological replicates, the mean and error bars represent the SEM. *, $P < 0.05$; **, $P < 0.01$; ***, $P < 0.001$.

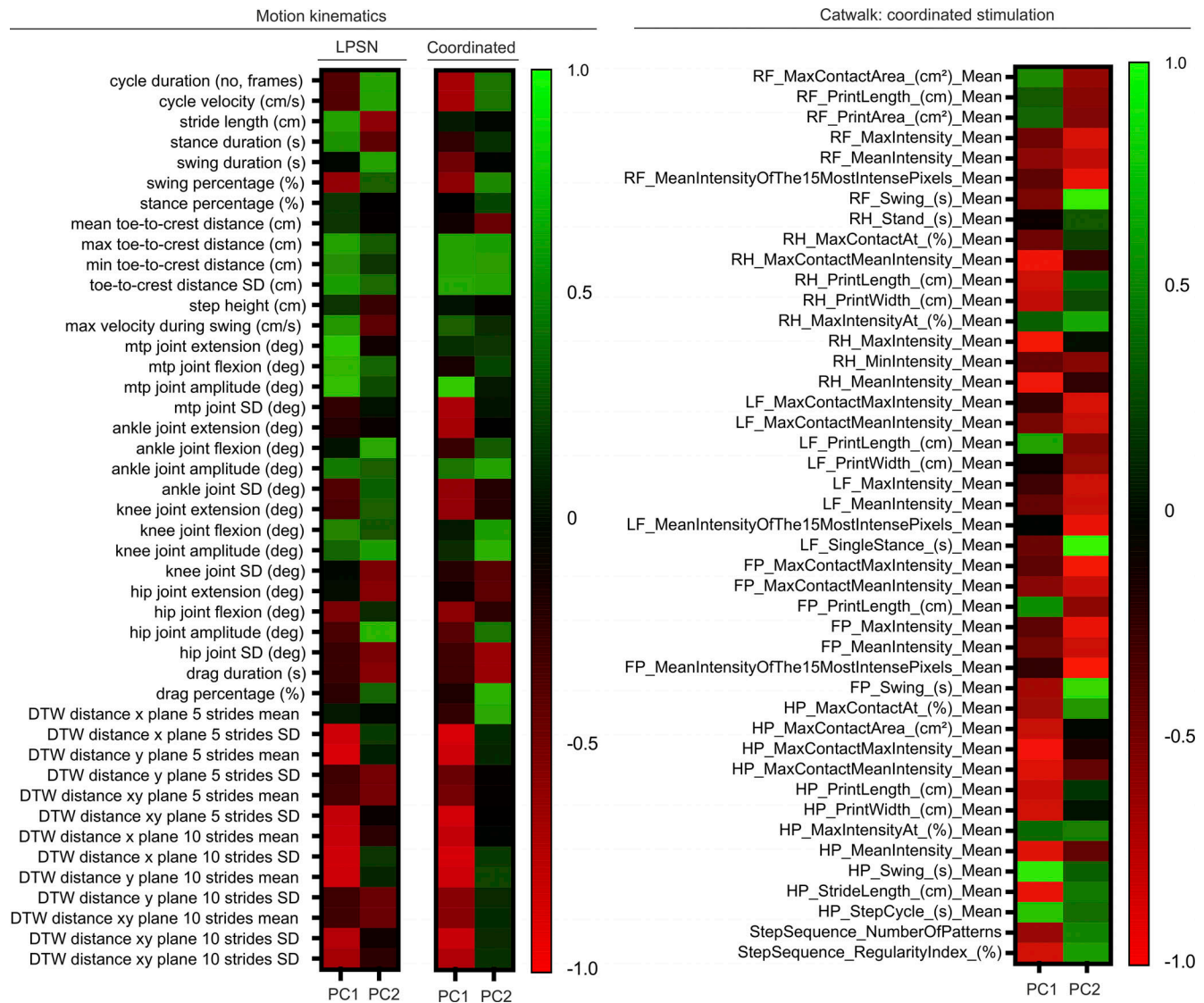


Figure S5. **Parameter loadings of principal components used for kinematic and CatWalk analysis.** Heatmaps of parameter loadings per principal component, showing changed parameters between control and LPSN stimulation (left, LPSN) and between CST, LPSN, and coordinated stimulation for motion kinematics analysis (left, Coordinated). Heatmap of parameter loadings per principal component, representing a subset of the correlated parameters between control and combined stimulation for CatWalk analysis (right).